Integrative Biology

PAPER

Cite this: *Integr. Biol.*, 2017, 9, 810

A multiscale study of the role of dynamin in the regulation of glucose uptake†

Raphaël Trouillon,[a] M. Cristina Letizia,[a] Keir J. Menzies,[‡b] Laurent Mouchiroud,[c] Johan Auwerx,[c] Kristina Schoonjans[b] and Martin A. M. Gijs*[a]

Received 20th January 2017,
Accepted 9th August 2017

DOI: 10.1039/c7ib00015d

rsc.li/integrative-biology

Glucose uptake in muscle cells in response to insulin is a fundamental mechanism for metabolism. The inability of cells to mobilize the specific glucose transporter GLUT4 is believed to be at least partially accountable for diseases, like diabetes, where cells do not respond to an insulin stimulus. In this work, a microchip is used to detect electrochemically glucose uptake from C2C12 myoblasts cultured on a patch of paper upon exposure to insulin. More importantly, the data suggest a new role for dynamin, a molecular motor which would be involved in GLUT4 translocation by facilitating exocytosis. It is also shown *in vivo* that dynamin is involved in the response to glucose in a completely distinct organism, namely the nematode *Caenorhabditis elegans*. The new mechanism for dynamin could therefore be more generally relevant *in vivo* and may play a role in insulin resistance.

Insight, innovation, integration

Developing new quantitative techniques and *in vivo* or *in vitro* models are crucial steps to extend our understanding of life sciences and to facilitate biomedical research. In this article, a versatile microfluidic system, fitted with an electrochemical sensor, is used to investigate glucose uptake from artificial tissues built on paper. The fundamental finding that dynamin is involved in this process was further extended in an organism-on-a-chip system, thus showing that dynamin also controls the response of *C. elegans* to high glucose levels. Overall, beyond the importance of the biological results, this work shows that carefully designed bioanalytical microsystems allow for the study of a specific phenomenon at a wide range of samples.

Introduction

Owing to the complexity of life, a reductionist approach is not always possible in life sciences.[1] This raises the issue of the relevance of models[2] of human physiology, which is currently considered as a cause for the high attrition rate in pharmacological research,[3] thus stressing the need for the development of new high predictive models.[4] One possible approach is the development of *in vitro* models[5] that closely mimic the functions of a human organ, such as organs-on-a-chip,[6] to facilitate research and preclinical benchmarking. Through the use of human cell lines and primary cell samples, one could expect obtaining an *in vitro* system with high reproducibility and similarity to humans, thus strengthening the preclinical assay validity of the drug. However, cell models are themselves limited as they lack, for instance, the behavioral response of a whole organism. To address this limitation, chips that can harbor whole organisms have been reported.[7] In this perspective, it is expected that the parallel use during preclinical assays or laboratory research of new tools focused on multiscale interrogation of a given biological phenomenon, *i.e.* at the molecular, tissue, and whole organism levels, could help providing a better mapping and improve the predictive value of these preliminary assays.

Recent developments in micro-engineering and cell-based assays have paved the way for a new generation of devices allowing for such dynamic measurements. Even though fluorescent[8] and microscopic techniques are the primary analytical modalities in this format, electrochemistry[9] is an ideal analytical method for such applications,[10] because of its high suitability to miniaturization and quantitative, dynamic experimentation. Owing to its versatility,

[a] *Laboratory of Microsystems, Ecole Polytechnique Fédérale de Lausanne, EPFL-STI-IMT-LMIS2, Building BM, Station 17, CH-1015 Lausanne, Switzerland. E-mail: martin.gijs@epfl.ch*
[b] *Laboratory of Metabolic Signaling, Ecole Polytechnique Fédérale de Lausanne, EPFL-SV-IBI-UPSCHOONJANS, Station 15, CH-1015 Lausanne, Switzerland*
[c] *Laboratory of Integrative and Systems Physiology, Ecole Polytechnique Fédérale de Lausanne, EPFL-SV-IBI-LISP, Station 15, CH-1015 Lausanne, Switzerland*

† Electronic supplementary information (ESI) available: Further details on the experimental methods, additional experimental results on the C2C12 glucose uptake and worm mobility assays. See DOI: 10.1039/c7ib00015d

‡ Present address: Interdisciplinary School of Health Sciences, University of Ottawa Brain and Mind Institute and Centre for Neuromuscular Disease, K1H 8M5, Ottawa, Canada.

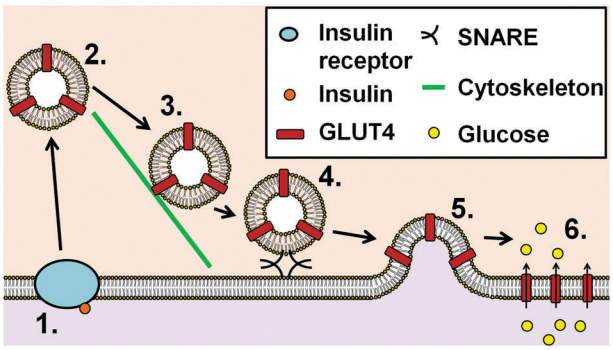

Fig. 1 Mechanism of GLUT4 mobilization and exocytosis in response to insulin:[25,26] the insulin receptor is stimulated (1) triggering an intracellular cascade (2) that induces GLUT4 storage vesicles trafficking (3), docking (4) and fusion with the membrane (5) *via* SNARE complexes. This results in membrane translocation of GLUT4 and glucose uptake (6).

unparalleled temporal resolution (typically in the order of the ms)[11] and the possibility to modify the electrode surface,[12–14] especially with enzymes,[15] electrochemical detection has been used in a wide variety of sample formats, such as single cells,[16–18] excised tissue,[19] *in vivo*[20] in vertebrate[21] and invertebrate[22] animals, artificial tissues[23] or biofluids.[24]

In this context, we report here the use of microfluidic/electrochemical systems to study glucose uptake, which is a critical process in metabolism. In a healthy individual, insulin is released to stimulate the uptake of glucose in muscles through specialized transporters, typically the insulin-responsive glucose transporter GLUT4 in mammals. However, the expression of the GLUT4 on the cell membrane followed by glucose uptake can be impaired, leading to the reduced response of muscle cells to insulin signaling.[27] Impaired mobilization of glucose transporters has been suggested to be a possible cause for diabetes mellitus type 2.[26] Fig. 1 summarizes the pathway leading to glucose uptake upon exposure to insulin.[25] The latter binds to its membrane receptor on a muscle cell, thus triggering an intracellular kinase cascade leading to the mobilization of intracellular GLUT4 storage vesicles (GSV). These GSV are translocated to the rim of the cell, where they can tether and fuse with the cell membrane following an exocytosis process. This allows for the integration of the GLUT4 transporters into the membrane, where they can take up glucose. The GLUT4 are re-integrated, mostly *via* clathrin-mediated endocytosis, in 10–20 minutes (half-life 4 to 20 minutes depending on the cells and conditions).[28,29]

In this work, we investigated the links between glucose uptake, *via* GLUT4 exocytosis, and dynamin. Dynamin[30] is a molecular motor normally involved in endocytosis but also found to contribute to exocytosis[31] through the dilation of the fusion pore,[32] as exposure to the selective inhibitor dynasore[33] was found to block exocytosis. We first quantified the insulin-induced glucose uptake in C2C12 myoblasts cultured on paper patches. We could observe a decrease in glucose uptake when the GTPase activity of dynamin is inhibited by dynasore. Secondly, fluorescent labelling of the membrane GLUT4 revealed that the translocation of GLUT4 to the membrane is also inhibited. Thirdly, owing to the limited relevance of cell models, an *in vivo* approach was chosen to investigate the translation of the biochemical findings in a more complex system. The nematode *C. elegans* was used as a whole body model. A custom chip allowed for the quantitative analysis of the nematodes' behavior, hinting that dynasore alters worms' response to high glucose exposure.

Results

Description of the device

The system is presented in Fig. 2A, and is adapted from a similar system, previously reported.[23] The bio-sample (*vide infra*) is maintained in the sample chamber and can be exposed to different streams of buffers and reactants. In all the experiments detailed here, the flow rate Q was 1 μl s^{-1}. This value allows for relatively fast experiments (about 5–10 minutes) without damaging the sample.[23] Downstream of the sample chamber is a detection chamber containing a 3-electrode system embedded into a syringe needle (Fig. 2B). The sensor was modified with glucose oxidase, following an adaptation of a method reported by others,[34] to allow

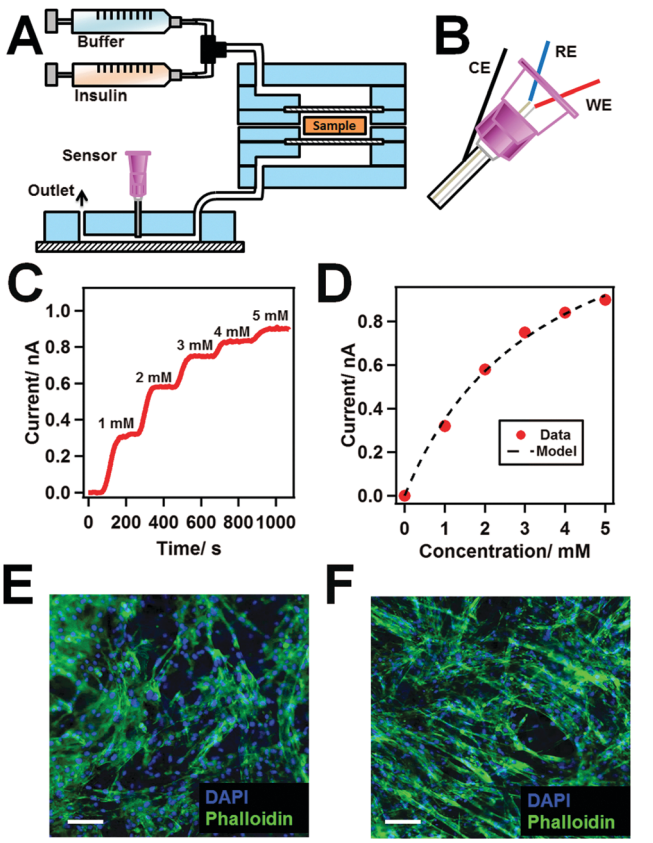

Fig. 2 Description of the electrochemical setup. (A) Scheme of the system, with the input syringes, the sample chamber and the sensing chamber containing the electrochemical sensor shown in more detail in (B) with its 3-electrode arrangement: counter (CE) pseudo-reference (RE) and working (WE) electrodes. (C) Typical calibration trace (Q = 1 μl s^{-1}), each step corresponds to a 1 mM increment, and (D) the associated calibration curve, fit with a Michaelis–Menten model. (E and F) Fluorescence microscopy images of C2C12 cells with stains for the nuclei (DAPI) and actin (phalloidin) components, grown on a paper patch for (E) 24 hours or (F) 5 days. Scale bars: 100 μm.

for the specific detection of glucose, and calibrated inside the chip (Fig. 2C). The resulting calibration curve showed the typical shape of a Michaelis–Menten reaction kinetic (Fig. 2D, see eqn (1)). The sensor used here is a first generation glucose sensor, *i.e.* ambient oxygen is used as a redox mediator.[15] The typical calibration curve does not significantly saturate in the considered range, and the Michaelis–Menten constant characterizing the saturation of the curve was in the 10 mM range (median 21 mM; 1st–3rd quartiles: 15–93 mM for 11 measurements). This shows that oxygen concentration is not the limiting factor in this setup, even for high glucose concentrations. Furthermore, the purpose of this work is to enclose cells in the system. The typical oxygen consumption of a cell is in the 10 amol s^{-1} $cell^{-1}$ range.[35] As 50 000 cells are typically used for our assay, for $Q = 1$ µl s^{-1}, this corresponds to a drop in oxygen concentration of ~1 µM, less than 1% of the concentration of the buffer in equilibrium with the atmosphere (250–300 µM),[35] in agreement with experimental observations for comparable cells density and Q.[36] Additionally, a large fraction of the system is made of PDMS, which is oxygen permeable, and the duration of the experiments is short. For these reasons, our assays are not limited by oxygen deficit.

Cells-on-paper samples

Even though slices of excised tissue are powerful models for bioanalysis, they can complicate the process as they originate from live animals. As a consequence, we chose to use a cells-on-paper approach where cells are cultured in a matrix of biopolymer on a piece of filter paper.[37] The resulting sample is economical, sturdy, easy to prepare and can be observed with fluorescent staining and epifluorescence microscopy. Despite cellulose autofluorescence, the topology of the sample can be observed, revealing the formation of a dense network of C2C12 cells 24 hours after cell seeding (Fig. 2E). Furthermore, the cells can be cultured for several days. As shown in Fig. 2F, after 100 000 cells were deposited on the patch and cultured for 5 days, the cells reorganized into bundles, a structure typical of an actual muscle. This preliminary result is not further investigated in this work, as cells were maintained on paper overnight, but nevertheless shows the wide capabilities of cells-on-paper techniques.

On-chip insulin-induced glucose uptake

The effect of insulin exposure can be observed directly, on chip, as shown in Fig. 3A. Here, a cell sample was placed in the chamber, the system was assembled and a stream of HEPES buffer containing 5 mM of glucose was flowed in the system. The sensor was poised at 0.7 V to allow for detection of glucose. Once the sensor response was stable, a solution of insulin (at 10 µg ml^{-1}) in HEPES buffer was injected into the system. The time axis is adjusted to take into account the dead volume, so that $t = 0$ s corresponds to the introduction of the insulin solution inside the sensing chamber. If 500 000 cells on a paper patch are positioned inside the device, a clear decrease in the current signal can be observed, starting after ~50 s and reaching a plateau after ~200 s. In this case where a high density of cells is seeded, this corresponds to a variation in glucose concentration at $t = 250$ s, $\Delta[\text{glucose}]_{250s}$, of −1.5 mM.

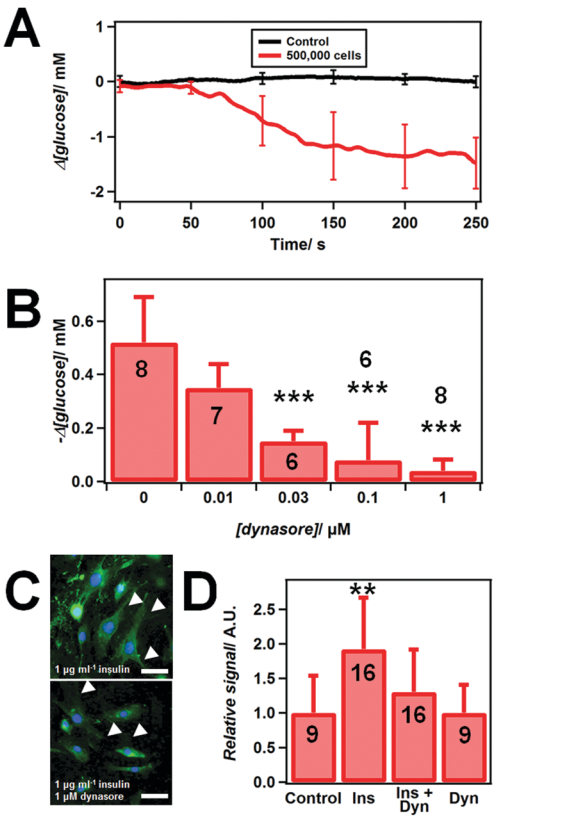

Fig. 3 Effect of dynamin inhibition in C2C12 cells. (A) Variations in [glucose] for 500 000 cells seeded on a patch exposed to 10 µg ml^{-1} insulin at $t = 0$ s ($n = 3$; control $n = 4$, obtained when no cells-on-paper sample is present in the system, $Q = 1$ µl s^{-1}). (B) Dose effect of dynasore on the magnitude of glucose uptake (50 000 cells per patch exposed to 1 µg ml^{-1} insulin, $Q = 1$ µl s^{-1}). The n value is indicated on each bar. (C) Fluorescent labelling of the membrane protein GLUT4 in C2C12 cells stimulated with 1 µg ml^{-1} insulin in the absence (top) or presence (bottom) of 1 µM dynasore. Scale bars: 50 µm. (D) Relative signal obtained from the fluorescent labelling of the membrane GLUT4 with 1 µg ml^{-1} insulin (Ins) and/or 1 µM dynasore (Dyn). $^{**}p < 0.01$; $^{***}p < 0.001$ in comparison to control on panels B (no dynasore) and D (no dynasore, no insulin).

In the control case, *i.e.* if the sample chamber is empty, no clear decrease in current is observed, revealing that insulin alone does not elicit an electrochemical response. In a previous study, the presence of the paper patch alone, without cells, did not impact the measurements.[23] As presented in the ESI,† the effects of the number of cells seeded in the sample and insulin concentration were investigated. As expected, the magnitude of $\Delta[\text{glucose}]_{250s}$ increased with both these parameters. More importantly, this study established that using 50 000 cells exposed to 1 µg ml^{-1} insulin is sufficient to obtain a strong glucose uptake signal, suitable for the study of pharmacological interferences. It was also found that no significant glucose uptake is recorded if no insulin is injected in the chip, in the presence of cells.

Effect of dynasore on insulin-induced glucose uptake

In the light of the mechanism presented in Fig. 1, most of the exocytosis machinery encountered for instance during neuronal

communication, such as the SNARE complex, the synaptotagmins and Ca^{2+} gradients, is also involved in this mechanism in muscle cells.[25] As a consequence, other molecules involved in exocytosis should also be considered as actors of insulin response.

Here, 50 000 C2C12 cells were exposed to 1 μg ml^{-1} of insulin for different concentrations of dynasore. Dynasore is a selective inhibitor of the dynamin family that blocks their GTPase activity[33] and was found to inhibit exocytosis.[23] A clear decrease in the magnitude of $\Delta[glucose]_{250s}$ is observed (Fig. 3B, $p = 3.1 \times 10^{-7}$, one-way ANOVA, 99.8% statistical power for $p = 0.001$), revealing an inhibition of glucose uptake as the GTPase activity of dynamin is blocked. The uptake was almost completely blocked for dynasore concentrations above 0.1 μM (for 0.1 μM, $p = 4 \times 10^{-4}$, 85% statistical power for $p = 0.001$; for 1 μM, $p = 3.0 \times 10^{-6}$, 92% statistical power for $p = 0.001$). This decrease was also concentration-dependent, with an IC50, defined as the dose required to obtain 50% of the maximal inhibition, determined to be ~0.02 μM. Importantly, the insulin initially triggers GLUT4 exocytosis through binding to its specific receptor, a transmembrane receptor tyrosine kinase, thus triggering a phosphorylation cascade.[38] Inhibiting the GTPase activity of dynamin is not expected to hinder this pathway.[33] Furthermore, the short (~5 min) preincubation time in dynasore solution before the experiment hints that complex interactions (post-translational modifications, alterations of protein expression, *etc.*) are unlikely, and that the observed phenomena mostly arise from dynamin inhibition. Further experiments could eventually focus at using cell mutants or siRNA. Dynasore was nevertheless chosen here owing to its fast action, and its ability to block dynamin in an un-modified sample, as dynamin mutants can show lower viability, defects, erratic behavior and diverge strongly from the control case.[39] A recent study published by others also report that new dynasore inhibitors also block exocytosis, thus showing that this effect is not an artifact of dynasore, but a reasonable indication that dynamin is also involved in vesicular release.[40]

As GLUT4 is expected to be endocytosed after 10–20 min, the observed glucose uptake should eventually go back to baseline if the insulin stimulation is removed. However, this case was not considered here.

Effect of dynasore on GLUT4 membrane translocation

To confirm that the reduced glucose uptake can indeed be attributed to impaired GLUT4 exocytosis when dynamin is inhibited by dynasore, the surface expression of GLUT4 was observed. The samples were stained with an anti-GLUT4 antibody (Fig. 3C), targeting an extracellular epitope of GLUT4. The procedure was performed on intact cells to avoid staining intracellular GLUT4. The cells were then permeabilized and stained with DAPI to allow for easy identification of the cell nuclei. When dynamin is functional, after incubation with insulin, a strong GLUT4 fluorescence can be observed, thus hinting a high density of transporters on the surface. However, if the cells have been pre-incubated with dynasore, the GLUT4 signal is reduced.

To quantify this reduction, the same experiment was performed, with fluorometry rather than microscopy, leading to a different and independent set of measurements (Fig. 3D, $p = 0.001$ for a one-way ANOVA test, 85% statistical power for $p = 0.01$). In this case, the GLUT4 signal increases strongly over control if the cells are incubated with insulin alone ($p = 5 \times 10^{-2}$, 93.2% statistical power for $p = 0.01$). This increase is abolished by co-incubation with dynasore, thus confirming that dynamin is critical for the surface expression of GLUT4 upon insulin stimulation.

Nematode glucose content

The previous results describe the role in dynamin in GLUT4 translocation in a cell model, but do not provide information regarding the translation of these findings to organisms. To investigate this possibility and establish whether the dynamin/GLUT4 interaction can still be formulated as a viable hypothesis *in vivo*, the nematode *C. elegans* was used as model, owing to its ease of use and maintenance, and also to the high conservation of the glucose and insulin pathways from mammalian organisms.[41] The purpose of this work is now to observe whether the findings of the previous sections can be extended to this organism, *i.e.* whether dynasore interacts or inhibits glucose uptake or behavioral responses to glucose.

Unsynchronized populations of ~2700 *C. elegans* were exposed to high (200 mM) glucose levels,[42] without or with 1 μM dynasore, lysed and the total glucose content of the lysate was quantified electrochemically (Fig. 4A, $p = 0.0012$, one-way ANOVA, 98% statistical power for $p = 0.01$). From this dataset, it appears clearly that dynasore blocked the accumulation of glucose in the worms, thus supporting the hypothesis that dynasore stopped glucose uptake ($p = 0.006$, 84% statistical power for $p = 0.01$). This result shows that the role of dynamin in glucose uptake translated well to complex, whole organism models, and strengthens the relevance of the analysis.

Nematode mobility assay

To extend these results to an *in vivo* situation, the effects of dynasore and glucose exposure to the nematode *C. elegans* were further studied. A microfluidic chip (Fig. 4B) allowing for the injection and selection of adult worms was used to expose a few worms to a constant flow ($Q = 30$ nl s^{-1}) of buffer, without or with drugs.[43] A video was captured before and after exposure, converted to binary and differentiated to extract a mobility score. It was found that increasing concentrations of glucose reduce the mobility (Fig. 4C), with a maximal drop in mobility of 50% reached for 200 mM ($p = 1.6 \times 10^{-5}$ *versus* 0 mM glucose). High glucose concentrations are known to have deleterious effects on nematodes lifespan[44] or to provoke oxidative stress.[45] A concentration of 200 mM glucose was chosen for the study to maximize the effect of the treatments.

The effects of increasing doses of dynasore, in presence or absence of glucose, are reported in Fig. 4D ($p = 1.9 \times 10^{-9}$ overall, one-way ANOVA, 99.9% power for $p = 10^{-5}$). The results of Student's *t*-test on this dataset are presented in the ESI.† In the absence of glucose, the mobility decreases with increased dynasore concentrations. This agrees well with a toxic effect *in vivo* of dynasore at high concentrations. However, the nematodes seem to recover some of their mobility upon removing of the dynasore,

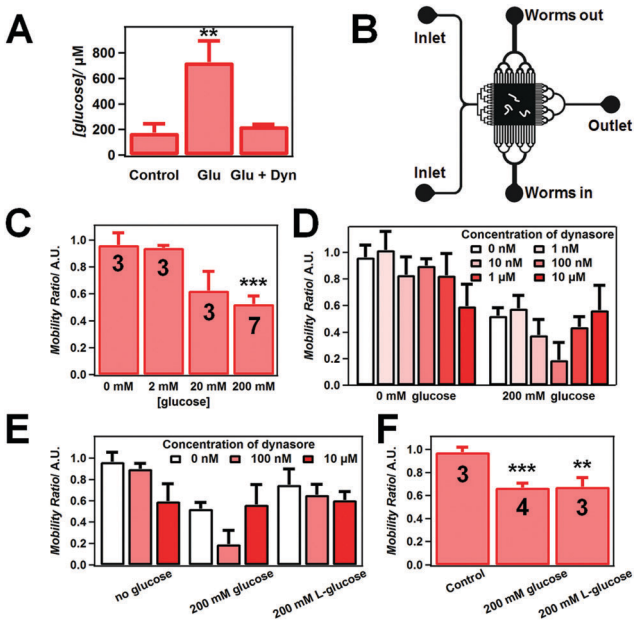

Fig. 4 Effects of glucose and dynasore on *C. elegans* glucose uptake and mobility. (A) Total glucose content measured electrochemically in worm lysates after exposure to 200 mM glucose, without (Glu) or with 1 µM dynasore (Glu + Dyn) and control without dynasore or glucose (n = 3 for each case, each repeat corresponds to the lysate of ~2700 worms). (B) Scheme of the microfluidic chip, showing the inlets and outlets allowing for the precise control of the chemical environment. The side of the square chamber measures 2 mm. Variations in mobility score for (C) different levels of glucose (the n value is mentioned in each bar) and (D) different levels of dynasore, for 0 and 200 mM of glucose. Variations in mobility score (E) for different enantiomers of glucose and different levels of dynasore and (F) for nematodes treated with *dyn-1* RNAi (all the worms used for this dataset were RNAi-treated). $^{**}p < 0.01$; $^{***}p < 0.001$ in comparison to control (panel A) or to the no glucose control case (panels C and F). For panels D and E, the n and p values are reported in ESI.†

indicating a reversibility of its action (see ESI†). The effect of dimethyl sulfoxide (DMSO), the vehicle in which dynasore was dissolved, in the worm response was investigated (n = 1 chip for each case). The highest concentration of dynasore used here corresponds to 0.01% DMSO, which was not found to alter the response of the worms in the absence (mobility ratio 0.89) or presence of 200 mM glucose (mobility ratio 0.52), hence showing the phenomena reported here are not induced by DMSO exposure.

In the presence of 200 mM glucose, the dose response to dynasore changes dramatically and becomes U-shaped. Low concentrations (up to 100 nM) seem to increase the observed glucose toxicity, the lowest mobility being recorded for 100 nM. However, if the dynasore level is increased above this 100 nM limit, the mobility increases too, up to the levels of mobility observed in the absence of glucose with 10 µM dynasore. This finding hints that high dynasore levels cancel the effect of glucose, possibly by blocking GLUT4 exocytosis and glucose uptake. The increased toxicity of low concentrations of drugs could be explained by a differential inhibition of the endocytotic and exocytotic pathways, as discussed below.

L-Glucose, an enantiomer of D-glucose (D-glucose is otherwise referred to as glucose in the text) that cannot enter glycolysis was used to investigate the specificity of glucose in the observed variations in mobility. L-Glucose has a low affinity with GLUT4 in contrast to glucose[46–48] and was previously found to show none of the typical harmful effects of glucose on *C. elegans*: the lifespan[44] and egg laying rate[49] were unaffected, and it displayed no toxicity in glucose-sensitive mutants.[50] This molecule was used to disentangle the physical (osmolarity, viscosity) and the enzymatic, metabolic or biological effects of the treatments (Fig. 4E, $p = 6.9 \times 10^{-5}$, one-way ANOVA, 88% statistical power for p = 0.001). Exposure to 200 mM L-glucose decreased the worm mobility in a smaller magnitude than glucose (p = 0.004, mobility ratio 0.75 for L-glucose *vs.* 0.52 for glucose, 96.0% statistical power for p = 0.001). This drop can be attributed to the physical effect of the molecule, principally the increase in osmolarity, on the nematodes. From this result, it can be estimated that the ~48% drop in mobility due to glucose exposure is the sum of a ~25% decrease due to the different physical conditions and another ~23% drop in mobility that can be attributed the biological impact of high glucose, probably leading to higher oxidative stress.

The L-glucose tests were also repeated for different concentrations of dynasore. Interestingly, the U-shaped response previously observed in the presence of glucose is abolished, and the trend of the response was comparable to the one recorded when no glucose is added. This further supports that the specific response seen for the co-exposure to glucose and dynasore arises specifically from the biological activity of glucose in *C. elegans*, and that dynamin takes part to this phenomenon.

Finally, to confirm the specific role of dynamin inhibition, worms were fed with a *E. coli* bacterial strain which expresses the RNAi targeting *dyn-1*, the gene encoding the dynamin homolog present in *C. elegans* (Fig. 4F).[39] The decrease in mobility due to 200 mM glucose was less than for the untreated worms (p = 0.002, mobility ratio 0.67 for the RNAi *vs.* 0.52 for the untreated, 87% statistical power for p = 0.001). Additionally, the decrease in mobility was similar for both glucose enantiomers, thus showing that the bioactivity of glucose does not alter the behavior of these RNAi-fed worms. As with dynasore, inhibiting the activity of dynamin *via* RNAi feeding blocks the biological response to glucose. The specific inhibition of *dyn-1 via* RNAi also confirms that the improved mobility observed with high dynasore levels is not due to reduced mitochondrial fragmentation through the inhibition the dynamin-like DRP-1,[51] but indeed because of the lower glucose uptake, as shown by the direct measurement of the glucose content in worms (Fig. 4A).

Overall, this set of experiments further establishes the role of dynamin in glucose uptake, as its activity modulates the magnitude of the nematode response to glucose. Additionally, it also hints at complex whole organism effects, *e.g.* behavioral alterations, mediated by the altered biochemical status of the animal.

Discussion

The results presented in this article point at a critical role for dynamin in the ability of cells to uptake glucose upon insulin stimulation. Importantly, evidence for this was found *in vitro*

but also *in vivo*, by taking advantage of the ease of use of *C. elegans*. The role of dynamin in glucose uptake was observed at the cell level with fluorescent labeling of GLUT4, at the 'tissue' level with electrochemical glucose uptake tests, at the whole organism level with the quantitation of glucose in *C. elegans* and finally at the behavioral level, thus providing an extensive mapping of the role of dynamin. To the best of our knowledge, this report is the first demonstration that microchip technology can be used to address the same biological question at different scales, thus possibly paving the way for new approaches in bioanalysis.

The experimental findings, in agreement with the literature, underline the fundamental role of dynamin in exocytosis. Dynamin inhibition was found to block glucose uptake in myoblasts but also to prevent the translocation of GLUT4 to the membrane upon exposure to insulin. Dynasore blocked glucose uptake in *C. elegans*, thus showing that the cell results translate well to the organism scale, but also altered the behavioral response of the nematodes to high glucose levels. The use of *C. elegans* is here relevant, as the insulin pathway is well conserved from this nematode to mammals.[52] Altogether, these findings suggest that dynamin is involved in the response to insulin by mediating the membrane expression of GLUT4, probably by facilitating exocytosis, as previously reported in other systems.[31,32]

Fig. 5A and B describes the proposed mechanisms for the role of dynamin in the response of myoblasts to insulin stimulation. In the control case (Fig. 5A), once the GSV has been tethered to the surface, the SNARE complex can initiate the formation of the fusion pore. Dynamin can spontaneously form a coil around such nanotubes (even in presence of dynasore) and its GTPase activity could stiffen this scaffold,[32] thus countering opposite forces that apply a pressure on the pore and prevent its dilation, such as the actin cytoskeleton.[53] Once the pore is sufficiently dilated, the GSV fully opens and fuses with the cell membrane, thus allowing for the integration of the GLUT4 in the membrane and glucose uptake. On the other hand, if the GTPase activity of dynamin is blocked (Fig. 5B), the dynamin coil cannot scaffold the pore and promote its dilation. The lipid nanotube initiated by the SNARE complex will therefore collapse and close, thus limiting the amount of GLUT4 that can be translocated to the membrane.

Another factor supporting this mechanism is the low dynasore IC50 observed in Fig. 3B. In a similar cells-on-paper system, the dynasore IC50 for neurotransmitter exocytosis was about one order of magnitude higher than the one observed here.[23] This is probably due to the different exocytotic modalities encountered in these systems. In the case of neurotransmitter release, the vesicle does not need to be fully integrated into the membrane. A significant body of literature actually supports that partial release, where the fusion pore is very short lived and just allows for the release of a fraction of the vesicle content, is the primary mode of neurotransmitter exocytosis.[54] In this case, a partially inhibited dynamin would not seriously impact exocytosis as long as the dynamin coil can maintain the pore open long enough to release the expected amount of transmitter. On the other hand, in the case of GLUT4 translocation, the GSV must open fully, and the contribution of dynamin is more important than in the partial release case. Hence, the system is more sensitive to dynamin inhibition, thus resulting in a lower IC50.

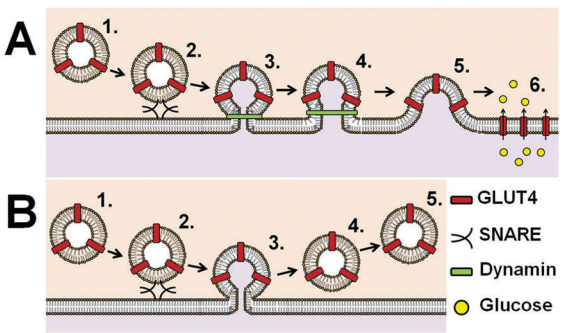

Fig. 5 Proposed mechanisms for the exocytosis of GLUT4 with (A) functional or (B) hindered (GTPase-deficient) dynamin activity.

The control of the GLUT4 levels on the cell membrane appears to result from the balance between exocytosis and endocytosis of the receptor.[55] As dynamin is involved in both mechanisms, the duration of the cell experiments was short (~5 min exposure to dynasore) to avoid artifacts due to impaired GLUT4 trafficking or depletion of the releasable GSV pool. Several reports have already underlined the importance of dynamin in the endocytosis of GLUT4.[55–57] In these longer-term cell studies, blocking or impairing the activity of dynamin was largely found to accumulate GLUT4 in the membrane, in the presence or absence of insulin, which may seem contradictory with our findings. This can be explained by the long (30 min) exposures to insulin principally considered in these reports, so that the initial response to insulin is not always resolved. Indeed, if adipocytes are transfected with a GTPase-deficient dynamin mutant, the level of membrane GLUT4 does not clearly change after a 5 min exposure to insulin, but increases dramatically for a 30 min incubation.[57] As the GLUT4 membrane concentration typically reaches a peak after 5 min in un-modified cells,[58] this fact indicates that dynamin inhibition does induce a slow accumulation of the transporter *via* inhibited endocytosis, but also impairs the capability of the cell to rapidly translocate GLUT4 in response to insulin, in agreement with a role for dynamin in GLUT4 exocytosis. It also hints that exocytosis is in this setup hindered, but endocytosis is completely blocked, thus leading to a slow rise in GLUT4 membrane concentration. This indicates that the endocytotic pathway is more dependent on dynamin viability than exocytosis. Similarly, if high levels of GTPase-deficient dynamin are expressed in rat adipose cells, the cells stop showing an ability to respond to insulin stimulation, despite a high basal level of membrane GLUT4.[59] Together with the data shown here, these studies reveal that dynamin is critical for both the translocation and removal of GLUT4 from the membrane, and that the endocytosis pathway is probably more sensitive to dysfunctions of dynamin than the exocytotic mechanisms.

These considerations were used to explain the U-shaped response observed on Fig. 4D. At low dynasore levels, the activity of dynamin is only partially inhibited. As the endocytotic pathway is more sensitive to this inhibition, the GLUT4 membrane

removal is decreased, thus leading to an enrichment of the membrane in GLUT4, and increasing glucose intake and the impact of glucose toxicity on the worms. As the dynasore concentrations, and the level of inhibition, increase, the exocytotic pathway becomes blocked too, thus blocking the GLUT4 translocation and reducing the ability of the nematodes to uptake glucose. This explains why the mobility recovers for higher concentrations of dynasore. The lifetime of GLUT4 in the membrane is typically 10 to 20 min,[28,29] a duration consistent with the *C. elegans* tests, but much shorter than the cell electrochemical assays. Therefore, the mobility assays account for both GLUT4 translocation and removal and describe the effect of dynamin inhibition on the basal membrane level of GLUT4. On the other hand, the C2C12 experiments focus at the insulin-stimulated changes and are too short ($\sim$4 minutes) to be strongly modified by endocytotic alterations. These differences explain why the U-shaped response seen in the nematode tests in the presence of dynasore is not observed for the cell measurements.

Several reports focused at the role of GLUT4 in diabetes mellitus type 2 have highlighted the possibility of a failure in the ability of the cell to translocate the GLUT4 from the GSVs to the membrane. Cells from diabetic patients typically show normal levels and expression of intracellular GLUT4[60] but only a small fraction of the GLUT4 is mobilized after exposure to insulin.[61] These reports therefore hint at a direct defect in the latest stages of GLUT4 translocation pathway. As a consequence, investigating the role of dynamin in the exocytosis of GLUT4 could be a working hypothesis for understanding the mechanisms of this disease.

Conclusion

Overall, in this article, a device for quantifying glucose uptake in cultured C2C12 cells was described. The system was fully characterized, and the glucose uptake data was found to be consistent with the current literature. More importantly, dynamin was identified as a critical factor in the translocation of GLUT4 to the cell surface, thereby mediating the response of myoblasts to insulin stimulation. This new role for dynamin was observed both at the cell and the whole organism levels using *C. elegans*. By considering the role of dynamin at the single cell level, as elucidated by labelling of the transporter, at the artificial tissue level, as evidenced with a functional assay which shows in real-time the actual glucose uptake, and at the whole organism level, as exemplified using behavioral and biochemical assays, the ubiquitous role of dynamin in exocytosis and in the overall regulation of molecular expression at the surface of the membrane was demonstrated. Furthermore, this new mechanism could shine some light on the causes of the impaired response of some cells to insulin and be relevant to the current research effort on diabetes.

Methods

Chemicals

The chemicals and reagents, of analytical grade, were all obtained from Sigma-Aldrich (unless stated otherwise) and used as received. All solutions were made using 18 MΩ cm water from a Millipore purification system. The HEPES physiological saline contained 150 mM NaCl, 5 mM KCl, 1.2 mM $MgCl_2$, 10 mM HEPES, and 2 mM $CaCl_2$. The solution pH was adjusted to 7.4 with concentrated (3 M) NaOH. The HEPES buffer was supplemented with 5 mM glucose or left glucose-free depending on the requirements, as detailed below. For the nematode culture and experiments, the nematode growth medium was prepared by autoclaving 975 ml H_2O supplemented with 3 g NaCl, 17 g agar, 2.5 g peptone and 1 ml cholesterol (5 mg ml^{-1} in ethanol). This mixture was completed with 1 ml 1 M CaCl, 1 ml 1 M $MgSO_4$ and 25 ml 1 M KPO_4 buffer. The S basal medium was prepared by adding 5.85 g NaCl, 1 g K_2HPO_4, 6 g KH_2PO_4, 1 ml cholesterol (5 mg ml^{-1} in ethanol) to 1 l H_2O. The S medium buffer was prepared by supplementing 1 l of S basal medium with 10 ml 1 M potassium citrate (pH 6), 10 ml trace metals solution, 3 ml 1 M $CaCl_2$, 3 ml 1 M MgSO.

Fabrication of the electrochemical chips

The fabrication of the chip was adapted from previously published methods and designs and were made using standard soft lithographic techniques.[23] The details of the fabrication steps are reported in the ESI.†

Preparation of the cell-seeded paper patches

The C2C12 cells were culture as described in the ESI† and seeded on paper patches using a published method.[23] The paper patches were cut in a sheet of paper (filter paper 114, Whatman, UK) with a 5 mm punch. The patches were cleaned successively by 10 min sonication in water and 70% ethanol, and then dried and sterilized in an oven at 120 °C for at least 6 hours. C2C12 cells were harvested by trypsinization and counted. After centrifugation, the cells were re-suspended in media at a concentration relevant of the experimental conditions. The cell solution was mixed, in a 1 : 1 ratio, with cold (4 °C) extracellular matrix (ECM) gel from Engelbreth-Holm-Swarm murine sarcoma. A 5 μl drop of the cell/ECM gel mixture was then deposited on each of the paper patches, which had been previously placed in individual wells of a 24-well plate. The initial cell density in the solution was adjusted so that the final number of cells per patch agrees with the experimental requirements (10 000 to 500 000 cells per patch depending on the experiment). After 2–5 min in the incubator to allow gelation, media was added to each well containing a seeded paper disk. The cells were incubated overnight before use.

For the dynasore experiments, a 100 mM stock solution was prepared by dissolving dynasore hydrate in DMSO (the molecular weight of anhydrous dynasore was used for this dilution). Even at the highest dynasore concentration considered in this study, the volume fraction of DMSO in the buffer was 10^{-4}, orders of magnitude below the reported toxicity levels.[62] DMSO was also reported to not affect cellular glucose uptake and GLUT4 translocation and activity in adipocytes below a volume fraction of $\sim$1%.[63] The cells were then exposed to HEPES buffer (5 mM glucose) containing the appropriate quantity of dynasore for 2–3 minutes.

The protocols for staining and imaging the cell samples are described in the ESI.†

Glucose uptake experiment

The calibration of the complete system was performed by injecting in the assembled system different concentrations of glucose in HEPES buffer at 1 μl s^{-1}, with the WE potential fixed at 0.7 V. In that configuration, the sample chamber was empty. The presence of a paper patch alone (*i.e.* without cells) was previously found to have no effect on the control measurements.[23] Briefly, one syringe was loaded with a 5 mM glucose solution, the other one with a 0 mM glucose solution. By modulating the Q for each syringe, different concentrations can be injected, as shown in Fig. 2C. For the actual experimental calibration, three points were tested (0, 2.5 and 5 mM) and the result was fit with a Michaelis–Menten model:[64]

$$I = I_{\max}\frac{[\text{glucose}]}{[\text{glucose}] + K_{\text{M}}} \quad (1)$$

where I is the measured current, $I_{\max}$ is the maximal current, and K_{M} is the Michaelis–Menten constant. The fitting parameters were found to differ for each sensor, but the median sensor sensitivity, in the linear range, approximated as $I_{\max}/K_{\text{M}}$ was 6.5 μA mM^{-1} cm^{-2} (1st–3rd quartiles: 5.5–15.1 μA mM^{-1} cm^{-2} for 11 measurements). The median limit of detection, defined as the glucose concentration reported by the sensor for a current equal to thrice the standard deviation of the baseline (evaluated here over 20 s, for a smoothed trace, as described below) was 4.2 μM (1st–3rd quartiles: 1.4–13.7 μM for 11 measurements). These parameters are in good agreement with reports from other groups for a similar type of sensor.

To perform cell measurements, the detection chamber is first filled with buffer, and the WE is poised at 0.7 V *vs.* pseudo Ag|AgCl until the recorded signal is stable. The buffer used for all these tests was 5 mM glucose in HEPES buffer. In the case of the experiments involving dynasore, the inhibitor was also added to all the buffers at the relevant concentration to avoid reversal of the inhibiting effect. Then, a paper patch loaded with cells is placed in the sample chamber. The two halves of the chip are assembled and held together using a custom holder. The sample chamber is connected to the two input 1 ml plastic syringes, placed in the syringe pump, using a T-junction and ∼10 cm of tubing. HEPES is injected into the system with Q = 1 μl s^{-1} to fill the chamber and remove air bubbles. The sample chamber is then connected, using ∼10 cm of tubing, to the detection chamber. HEPES is continuously injected at 1 μl s^{-1} for ∼1 min to flush away air bubbles, and the system is carefully checked for leaks. Once the system is ready, a stream of insulin (at the relevant concentration in 5 mM glucose in HEPES buffer) is injected and the recording of the electrochemical signal is initiated simultaneously. The experiments were carried out at room temperature, and the sampling frequency was 1 Hz.

As detailed elsewhere,[23] the dead-volume time T_{DV}, *i.e.* the delay between the injection of a plug of analyte and the time when it is detected by the potentiostat, is subtracted from the time axis, so that 0 s corresponds to the time when the stimulating buffer enters the detection chamber. In our setup, T_{DV} was typically in the 60 s to 100 s range. The traces were filtered with a binomial filter, over 11 points. The baseline is fitted with a decaying exponential and subtracted from the signal and converted to concentration using the calibration data. The section of the recorded data normally corresponding to the presence of insulin buffer in the chamber is not taken into account in the background fitting. The main parameter extracted from these data is the decrease in glucose concentration at t = 250 s, $\Delta[\text{glucose}]_{250\text{s}}$, which corresponds to the amount of glucose absorbed by the cells from the 5 mM buffer.

Worm mobility and glucose assays

The details of this procedure are reported in the ESI.† Briefly, for the mobility assay, the worms were maintained in a custom chip made using standard soft lithographic techniques. The variations in worm mobility were evaluated using a custom algorithm written in IgorPro (Wavemetrics, USA). For the glucose assays, the worms were lysed in acid and glucose levels were measured electrochemically.

Statistics

Where applicable, the data are reported as average ± standard deviation (SD), and the number of individual measurements is described using the notation n. A Shapiro–Wilk test was run on the different control datasets obtained in the study. The p-values obtained ($p > 0.25$ for all the control datasets) indicate that the normality hypothesis cannot be rejected. The validity of the normal distribution hypothesis was then confirmed by plotting Q–Q plots. Comparisons between two different datasets were performed with a two-tailed Student's t-test, or with a 1-way ANOVA in the case of more than 2 datasets, followed by a post-hoc two-tailed Student's t-test if further comparisons are required.

The statistical power of the different tests was computed for p = 0.01 or p = 0.001 depending on the p value returned by the statistical test. Overall, the study is well-powered (power typically 80% or higher) thus establishing the reliability of the data. More details on statistics and data processing are available in the ESI.†

Conflicts of interest

There are no conflicts of interest to declare.

Acknowledgements

Funding of this work was provided by the EPFL and the EU Ideas program (ERC-2012-AdG-320404). The authors thank the staff of the Center of Micro- and Nanotechnology at EPFL for assistance in the micro-fabrication processes. The group of Nikolaos Stergiopulos at EPFL is gratefully acknowledged for providing access to its cell culture facility. Dr Vincenzo Sorrentino (EPFL) is gratefully acknowledged for his assistance with the *C. elegans* experiments.

Notes and references

1 A. C. Ahn, M. Tewari, C.-S. Poon and R. S. Phillips, *PLoS Med.*, 2006, **3**, e208.
2 S. Perrin, *Nature*, 2014, **507**, 423–425.

3 J. W. Scannell, A. Blanckley, H. Boldon and B. Warrington, *Nat. Rev. Drug Discovery*, 2012, **11**, 191–200.
4 J. W. Scannell and J. Bosley, *PLoS One*, 2016, **11**, e0147215.
5 N. Picollet-D'hahan, M. E. Dolega, L. Liguori, C. Marquette, S. L. Gac, X. Gidrol and D. K. Martin, *Trends Biotechnol.*, 2016, **34**, 757–769.
6 P. Neuži, S. Giselbrecht, K. Länge, T. J. Huang and A. Manz, *Nat. Rev. Drug Discovery*, 2012, **11**, 620–632.
7 V. Sivagnanam and M. A. M. Gijs, *Chem. Rev.*, 2013, **113**, 3214–3247.
8 R. Davidsson, B. Johansson, V. Passoth, M. Bengtsson, T. Laurell and J. Emnéus, *Lab Chip*, 2004, **4**, 488–494.
9 A. J. Bard and R. L. Faulkner, *Electrochemical Methods: Fundamentals and Applications*, John Wiley and Sons, Hoboken, NJ, USA, 2nd edn, 2001.
10 R. Trouillon, M. I. Svensson, E. C. Berglund, A.-S. Cans and A. G. Ewing, *Electrochim. Acta*, 2012, **84**, 84–95.
11 R. Trouillon, Y. Lin, L. J. Mellander, J. D. Keighron and A. G. Ewing, *Anal. Chem.*, 2013, **85**, 6421–6428.
12 R. Trouillon, Y. Einaga and M. A. M. Gijs, *Electrochem. Commun.*, 2014, **47**, 92–95.
13 R. Trouillon, D. O'Hare and Y. Einaga, *Phys. Chem. Chem. Phys.*, 2011, **13**, 5422–5429.
14 R. Trouillon, Z. Combs, B. A. Patel and D. O'Hare, *Electrochem. Commun.*, 2009, **11**, 1409–1413.
15 J. Wang, *Electroanalysis*, 2001, **13**, 983–988.
16 R. M. Wightman, J. A. Jankowski, R. T. Kennedy, K. T. Kawagoe, T. J. Schroeder, D. J. Leszczyszyn, J. A. Near, E. J. Diliberto Jr and O. H. Viveros, *Proc. Natl. Acad. Sci. U. S. A.*, 1991, **88**, 10754–10758.
17 J. Wang, R. Trouillon, J. Dunevall and A. G. Ewing, *Anal. Chem.*, 2014, **86**, 4515–4520.
18 R. Trouillon and A. G. Ewing, *Anal. Chem.*, 2013, **85**, 4822–4828.
19 E. Bitziou, D. O'Hare and B. A. Patel, *Anal. Chem.*, 2008, **80**, 8733–8740.
20 G. S. Wilson and M. A. Johnson, *Chem. Rev.*, 2008, **108**, 2462–2481.
21 A. G. Ewing, J. C. Bigelow and R. M. Wightman, *Science*, 1983, **221**, 169–171.
22 S. Majdi, L. Ren, H. Fathali, X. Li and A. G. Ewing, *Analyst*, 2015, **140**, 3676–3686.
23 R. Trouillon and M. Gijs, *RSC Adv.*, 2016, **6**, 31069–31073.
24 T. Seppala, M. Scheinin, A. Capone and M. Linnoila, *Acta Pharmacol. Toxicol.*, 1984, **55**, 81–87.
25 J. Stöckli, D. J. Fazakerley and D. E. James, *J. Cell Sci.*, 2011, **124**, 4147–4159.
26 S. Huang and M. P. Czech, *Cell Metab.*, 2007, **5**, 237–252.
27 J. W. Ryder, J. Yang, D. Galuska, J. Rincón, M. Björnholm, A. Krook, S. Lund, O. Pedersen, H. Wallberg-Henriksson, J. R. Zierath and G. D. Holman, *Diabetes*, 2000, **49**, 647–654.
28 S. Shigematsu, A. H. Khan, M. Kanzaki and J. E. Pessin, *Mol. Endocrinol.*, 2002, **16**, 1060–1068.
29 L. J. Foster, D. Li, V. K. Randhawa and A. Klip, *J. Biol. Chem.*, 2001, **276**, 44212–44221.
30 G. J. K. Praefcke and H. T. McMahon, *Nat. Rev. Mol. Cell Biol.*, 2004, **5**, 133–147.
31 A. Anantharam, D. Axelrod and R. W. Holz, *J. Neurochem.*, 2012, **122**, 661–671.
32 R. Trouillon and A. G. Ewing, *ChemPhysChem*, 2013, **14**, 2295–2301.
33 E. Macia, M. Ehrlich, R. Massol, E. Boucrot, C. Brunner and T. Kirchhausen, *Dev. Cell*, 2006, **10**, 839–850.
34 N. Vasylieva, B. Barnych, A. Meiller, C. Maucler, L. Pollegioni, J.-S. Lin, D. Barbier and S. Marinesco, *Biosens. Bioelectron.*, 2011, **26**, 3993–4000.
35 B. A. Wagner, S. Venkataraman and G. R. Buettner, *Free Radical Biol. Med.*, 2011, **51**, 700–712.
36 G. Mehta, K. Mehta, D. Sud, J. W. Song, T. Bersano-Begey, N. Futai, Y. S. Heo, M.-A. Mycek, J. J. Linderman and S. Takayama, *Biomed. Microdevices*, 2007, **9**, 123–134.
37 R. Derda, A. Laromaine, A. Mammoto, S. K. Y. Tang, T. Mammoto, D. E. Ingber and G. M. Whitesides, *Proc. Natl. Acad. Sci. U. S. A.*, 2009, **106**, 18457–18462.
38 F. P. Ottensmeyer, D. R. Beniac, R. Z.-T. Luo and C. C. Yip, *Biochemistry*, 2000, **39**, 12103–12112.
39 S. G. Clark, D.-L. Shurland, E. M. Meyerowitz, C. I. Bargmann and A. M. van der Bliek, *Proc. Natl. Acad. Sci. U. S. A.*, 1997, **94**, 10438–10443.
40 E. Lasič, M. Stenovec, M. Kreft, P. J. Robinson and R. Zorec, *Biochim. Biophys. Acta, Gen. Subj.*, 2017, **1861**, 2293–2303.
41 K. D. Kimura, H. A. Tissenbaum, Y. Liu and G. Ruvkun, *Science*, 1997, **277**, 942–946.
42 G. Zhu, F. Yin, L. Wang, W. Wei, L. Jiang and J. Qin, *Integr. Biol.*, 2016, **8**, 30–38.
43 M. Cornaglia, L. Mouchiroud, A. Marette, S. Narasimhan, T. Lehnert, V. Jovaisaite, J. Auwerx and M. A. M. Gijs, *Sci. Rep.*, 2015, **5**, 10192.
44 S.-J. Lee, C. T. Murphy and C. Kenyon, *Cell Metab.*, 2009, **10**, 379–391.
45 A. Schlotterer, G. Kukudov, F. Bozorgmehr, H. Hutter, X. Du, D. Oikonomou, Y. Ibrahim, F. Pfisterer, N. Rabbani, P. Thornalley, A. Sayed, T. Fleming, P. Humpert, V. Schwenger, M. Zeier, A. Hamann, D. Stern, M. Brownlee, A. Bierhaus, P. Nawroth and M. Morcos, *Diabetes*, 2009, **58**, 2450–2456.
46 T. Kasahara and M. Kasahara, *Biochim. Biophys. Acta, Biomembr.*, 1997, **1324**, 111–119.
47 S. L. McMillin, D. L. Schmidt, B. B. Kahn and C. A. Witczak, *Diabetes*, 2017, **66**, 1491–1500.
48 R. C. Hresko, T. E. Kraft, A. Quigley, E. P. Carpenter and P. W. Hruz, *J. Biol. Chem.*, 2016, **291**, 17271–17282.
49 E. Teshiba, K. Miyahara and H. Takeya, *Biosci., Biotechnol., Biochem.*, 2016, **80**, 1436–1439.
50 E. Svensk, R. Devkota, M. Ståhlman, P. Ranji, M. Rauthan, F. Magnusson, S. Hammarsten, M. Johansson, J. Borén and M. Pilon, *PLoS Genet.*, 2016, **12**, e1005982.
51 R. Jagasia, P. Grote, B. Westermann and B. Conradt, *Nature*, 2005, **433**, 754–760.
52 M. Barbieri, M. Bonafè, C. Franceschi and G. Paolisso, *Am. J. Physiol.: Endocrinol. Metab.*, 2003, **285**, E1064–E1071.
53 R. Trouillon and A. G. Ewing, *ACS Chem. Biol.*, 2014, **9**, 812–820.
54 L. Ren, L. J. Mellander, J. Keighron, A.-S. Cans, M. E. Kurczy, I. Svir, A. Oleinick, C. Amatore and A. G. Ewing, *Q. Rev. Biophys.*, 2016, **49**, e12.

55 R. T. Watson, M. Kanzaki and J. E. Pessin, *Endocr. Rev.*, 2004, **25**, 177–204.
56 A. Volchuk, S. Narine, L. J. Foster, D. Grabs, P. D. Camilli and A. Klip, *J. Biol. Chem.*, 1998, **273**, 8169–8176.
57 A. W. Kao, B. P. Ceresa, S. R. Santeler and J. E. Pessin, *J. Biol. Chem.*, 1998, **273**, 25450–25457.
58 R. Govers, A. C. F. Coster and D. E. James, *Mol. Cell. Biol.*, 2004, **24**, 6456–6466.
59 H. Al-Hasani, C. S. Hinck and S. W. Cushman, *J. Biol. Chem.*, 1998, **273**, 17504–17510.
60 W. T. Garvey, L. Maianu, J. A. Hancock, A. M. Golichowski and A. Baron, *Diabetes*, 1992, **41**, 465–475.
61 W. T. Garvey, L. Maianu, J. H. Zhu, G. Brechtel-Hook, P. Wallace and A. D. Baron, *J. Clin. Invest.*, 1998, **101**, 2377–2386.
62 C.-C. Wang, S.-Y. Lin, Y.-H. Lai, Y.-J. Liu, Y.-L. Hsu and J. J. W. Chen, *PLoS One*, 2012, **7**, e33772.
63 M. Berenguer, J. Zhang, M. C. Bruce, L. Martinez, T. Gonzalez, A. A. Gurtovenko, T. Xu, Y. Le Marchand-Brustel and R. Govers, *Biochimie*, 2011, **93**, 697–709.
64 L. Michaelis and M. Menten, *Biochem. Z.*, 1913, **49**, 352.